Current oscillation of snake states in graphene *p-n* junction

Jiang-chai Chen,[1] X. C. Xie,[2] and Qing-feng Sun[1,*]
[1]*Institute of Physics, Chinese Academy of Sciences, Beijing 100190, China*
[2]*International Center for Quantum Materials, Peking University, Beijing 100871, China*
(Received 17 April 2012; published 19 July 2012)

Snake states in a six-terminal graphene *p-n* junction are investigated under a perpendicular magnetic field. The current oscillation with varying magnetic field appears due to the presence of snake states at the *p-n* interface. At a fixed magnetic field, the periodic properties of currents with respect to the geometric structures, such as the graphene ribbon width and the location of the incident terminal, are also shown. We extract the values of the width and the location corresponding to the maximums of the current and plot them versus their sequence number. They form a straight line, which shows that the oscillation is periodic. The periods decrease with increasing magnetic field. The order of magnitude of periods and their tendencies with varying a magnetic field are consistent with those predicted from semiclassical motions. Finally, for a smooth potential, the snake states still survive and the oscillation phase and the oscillation period with respect to the location of the incident terminal are almost unchanged, but the period with respect to the width of the ribbon is reduced.

DOI: 10.1103/PhysRevB.86.035429 PACS number(s): 72.80.Vp, 73.23.Ad, 73.40.Lq

I. INTRODUCTION

Graphene,[1–3] a single layer of carbon atoms packed in a honeycomb lattice,[4] has been extensively investigated since its successful isolation. The unique band structure of graphene has many unusual properties, such as its Hall conductance plateaus occurring at half-integer values[2,3] $4(n+1/2)e^2/h$ with the integer n denoting the Landau-level index. Recently, it was found that different carrier types as well as variable concentrations can be obtained experimentally by tuning the gate voltage or doping.[5–7] Thus, the dual-gated graphene devices, such as *p-n* and *p-n-p* junctions, are formed by connecting graphene ribbons with different carrier types.[5–11] These devices provide an effective medium to investigate some exotic phenomena, for instance, Veselago lensing[12,13] and relativistic Klein tunneling.[14,15]

In addition, in graphene, the quasiparticles of low energy have a unique linear dispersion and formally obey a Dirac-like equation as if they behave like the massless Dirac carriers.[4] Thus, the carriers can propagate through the interface between *n*-type and *p*-type regions in a graphene *p-n* junction as in Klein tunneling. If the incident angle is perpendicular to the interface, carriers pass through the interface without reflection, whereas the incident carriers at oblique angles are partially reflected.[15,16] The potential profile along the barrier can also affect the transmission probability of carriers. The smooth barrier is more efficient in reflecting carriers at an oblique incident angle.[16]

Furthermore, if a perpendicular magnetic field is applied for a graphene *p-n* junction, snake states are formed and zigzag along the *p-n* interface due to a change in the direction of the Lorentz force, which results from a sign change of charge carriers across the junction. Their classical trajectories curve back and forth along the *p-n* interface [see Fig. 1(b)]. Snake states in graphene have been proposed theoretically for inhomogeneous magnetic fields[17,18] as in a two-dimensional electron gas.[19,20] Very recently, the existence of the snake states was also indicated experimentally for a uniform magnetic field in a graphene *p-n* junction.[21]

In this work, a measurement is proposed to investigate snake states in a six-terminal graphene *p-n* junction under a perpendicular magnetic field [see Fig. 1(a)], from which more properties can be obtained. The carriers are injected from terminal 6, which couples to the device by a quantum point contact, so the incident carriers are a collimated beam.[22,23] The voltages of other terminals are set to zero and the currents are detected from each terminal. In a suitable magnetic field, currents flow out only from terminal 2 and terminal 3 due to the formation of edge states and the presence of a snake state at the *p-n* interface, and the currents oscillate as a function of the magnetic field. At a fixed magnetic field, the currents also exhibit oscillation behaviors with varying width of the graphene ribbon and the location of incident terminal 6, which clearly indicates the existence of snake states. These current oscillations are periodic and can exist in very large ranges of ribbon width and the location of incident terminal 6. The oscillation periods decrease with increasing magnetic field. In addition, the order of magnitude for these periods and their tendencies with varying magnetic field are the same as those of semiclassical motions, although they are not identical to each other. Finally, the snake states can exist even in smooth potential at the *p-n* interface. In particular, the smooth potential does not affect the oscillation phase or the oscillation period with respect to the location of the incident terminal, but it reduces the period with respect to the width of the ribbon. Experimentally, the above current oscillation can be detected by varying a magnetic field or moving the tip of a scanning tunneling microscope (STM) where a STM tip replaces the fixed terminal 6 as the incident terminal.

The rest of the paper is organized as follows. In Sec. II, we describe the model and give the details of our calculations. In Sec. III, we study the current oscillation of a snake state for a sharp-step-potential case. The oscillation period is investigated in Sec. IV. Section V is devoted to the case of the smooth potential. Finally, a brief conclusion is presented in Sec. VI.

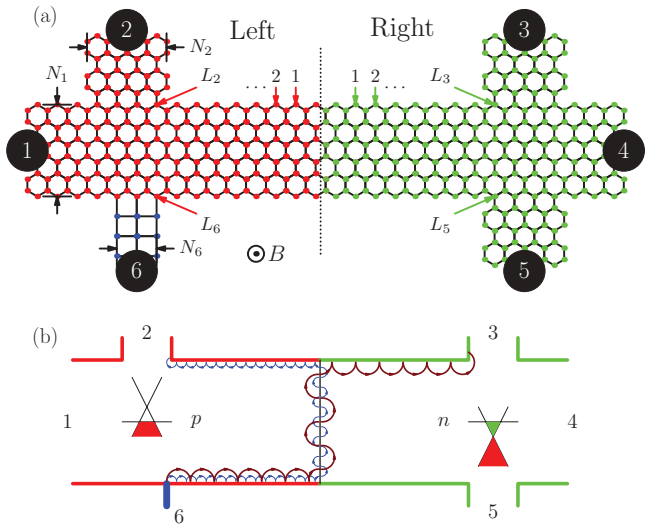

FIG. 1. (Color online) (a) The schematic diagram of a six-terminal graphene p-n junction under a perpendicular magnetic field. The left and right regions are separated by a dotted line. (b) The schematic diagram for two classical routes of the snake state in the above device (here the currents are incident perpendicularly at the p-n interface).

II. MODEL AND CALCULATION

A six-terminal graphene p-n junction under a perpendicular magnetic field is considered [as shown in Fig. 1(a)]. The left region contains terminals 1, 2, and 6 and the right region contains terminals 3, 4, and 5. The charge current is incident from terminal 6 into the device and then flows out from the other five terminals, whose voltages are set to zero. In order to collimate the current,[22,23] terminal 6 is very narrow to form a quantum point contact with the graphene ribbon. Here, a square lattice is adopted for terminal 6 to avoid the appearance of a gap for the armchair edge of the honeycomb lattice[24] in the case of a narrow terminal 6. In the tight-binding representation, the Hamiltonian of the device is given by[25–28]

$$H = \sum_i \epsilon_i a_i^\dagger a_i - \sum_{\langle ij \rangle} t e^{i\phi_{ij}} a_i^\dagger a_j, \tag{1}$$

where $a_i^\dagger$ and a_i are, respectively, the creation and annihilation operators at site i, and ϵ_i is the energy of the Dirac point (i.e., the on-site energy). We mainly focus on the sharp step potential, so ϵ_i is equal to E_L and E_R in the left and right regions, respectively. At last (in Sec. V), when the smooth potential is considered, ϵ_i between terminals 2 and 3 will be changed slowly, column by column. The second term in the Hamiltonian stands for the nearest-neighbor hopping. The effect of the magnetic field is addressed by the phase $\phi_{ij} = \int_i^j \mathbf{A} \cdot d\mathbf{l}/\boldsymbol{\phi_0}$ in the hopping term where $\mathbf{A} = (-yB,0,0)$ is the vector potential and $\phi_0 = \hbar/e$. The magnetic field B is applied to the whole device along the perpendicular direction.

By means of the Landauer-Büttiker formula at zero temperature, the current in lead p can be expressed as[27–29]

$$I_p = \frac{2e^2}{h} \sum_{q(\neq p)} T_{pq}(E_F)(V_p - V_q). \tag{2}$$

Here, $T_{pq}(E_F) = \mathrm{Tr}[\mathbf{\Gamma}_p \mathbf{G}^r \mathbf{\Gamma}_q \mathbf{G}^a]$ is the transmission coefficient from the lead q to p at the Fermi energy E_F, $\mathbf{\Gamma}_p(E_F) = i[\mathbf{\Sigma}_p^r(E_F) - \mathbf{\Sigma}_p^a(E_F)]$ is the linewidth function, $\mathbf{G}^r(E_F) = [\mathbf{G}^a]^\dagger = 1/[E_F\mathbf{I} - \mathbf{H}_c - \sum_p \mathbf{\Sigma}_p^r]$ is the retarded Green's function, and $\mathbf{H}_c$ denotes the Hamiltonian of the central region without the six terminals. The retarded self-energy $\mathbf{\Sigma}_p^r(E_F)$ due to the coupling to the lead p can be calculated numerically.[30] The voltage V_6 for incident terminal 6 is set to a small value V, and $V_q (q = 1, \ldots, 5)$ for other terminals are set to zero. Thus, the current I_p on each terminal can be obtained directly from Eq. (2).

In our simulation, we also set the Fermi energy at $E_F = 0$, the hopping energy $t(\approx 2.8$ eV) as the energy unit, $2e^2V/h$ as the current unit, and $E_L = -E_R$ (i.e., the barrier height is $2|E_L|$). In the following, we neglect the sign of the charge current. In fact, according to the above voltage bias, many carriers flow from terminal 6 into the device, and then flow from the device into the other five terminals. The effect of the magnetic field is addressed by the Peierls phase[31] BS/ϕ_0, where S is the area of a unit cell. Hence, the Peierls phase is taken as $2\phi = (3\sqrt{3}/2)a^2B/\phi_0$ for a honeycomb lattice and $(4/\sqrt{3})\phi$ for a square lattice, where $a \approx 0.142$ nm is the distance between two neighboring carbons. The size of device is assumed as follows. The width of terminals 1 and 4 is $(3N_1 - 1)a$; the width of terminals 2, 3, and 5 is $\sqrt{3}N_2a$; and the width of terminal 6 is $\sqrt{3}N_3a$. In Fig. 1(a), $N_1 = 3$, $N_2 = 4$, and $N_6 = 2$. The locations of terminals 2, 3, 5, and 6 are denoted by L_2, L_3, L_5, and L_6, respectively, as seen in Fig. 1(a).

III. CURRENT OSCILLATION OF SNAKE STATES FOR THE SHARP STEP POTENTIAL

In Fig. 1(b), the classical figure of snake states in a six-terminal p-n graphene junction is plotted, where the carriers are holes in the left region and electrons in the right region (i.e., $E_L = -E_R > 0$). In the beginning, the holes are injected from terminal 6 and skip along the boundary until they arrive at the p-n interface. Then, snake states are formed and zigzag along the interface due to the sign change of the Lorentz force for holes and electrons across the junction. There are two ways to control the final route of snake states toward the left or right direction: (i) If the geometrical structure of a device is fixed, the magnetic field determines at which terminal the snake states arrive. Two classical routes under different magnetic fields are shown in Fig. 1(b), where one flows into terminal 2 and another into terminal 3. (ii) If the magnetic field is a constant, the final terminal that snake states reach can be determined by changing the geometrical structure, such as the width of the ribbon, N_1, and the location of incident terminal 6, L_6.

At first, we fix the geometrical structure of the device with a sharp step potential and investigate the charge current with varying the magnetic field as seen in Figs. 2(a) and 2(b). Owing to current conservation, $I_6 = I_1 + \cdots + I_5$. According to the incident current I_6, several regions appear as increasing magnetic field, which are separated by some special magnetic fields, such as ϕ_1 and ϕ_2. In Figs. 2(c) and 2(d), the band structures are depicted in magnetic fields ϕ_1 and ϕ_2. In ϕ_1, the Fermi energy just meets the second-hole Landau level of

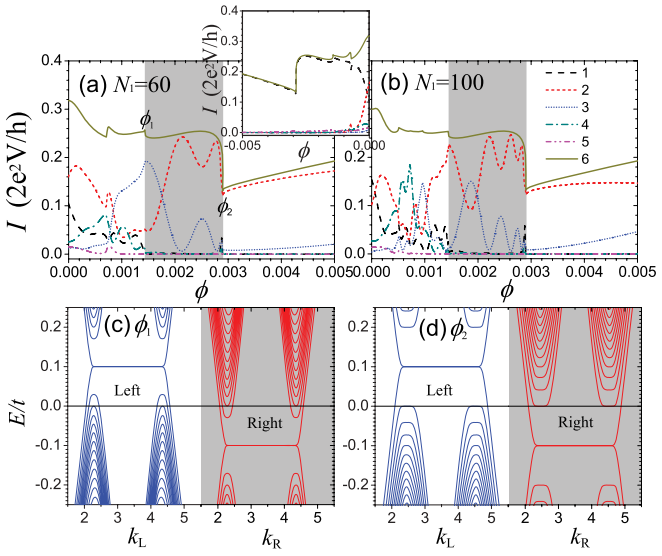

FIG. 2. (Color online) The charge currents I_n ($n = 1,2,\ldots,6$) as a function of magnetic field ϕ with different widths of ribbon, (a) $N_1 = 60$ and (b) $N_1 = 100$. The legend in (b) is for the panels (a) and (b). Inset of (a): inverse magnetic field for (a). (c,d) Energy-band structures for selected magnetic fields in (a): (c) ϕ_1 and (d) ϕ_2. Here the left and right subplots correspond to the energy-band structures for the graphene ribbons of the left side and right side of the p-n junction, respectively. Other parameters are $N_2 = 60$, $N_6 = 3$, $L_2 = L_3 = L_5 = L_6 = 20$, and $E_L = -E_R = 0.1$.

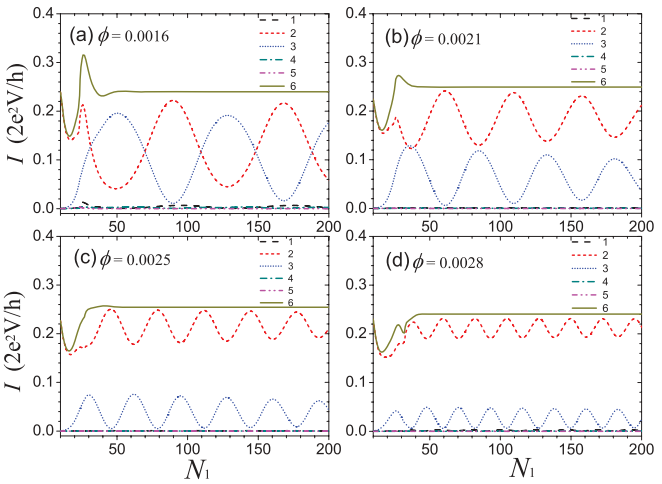

FIG. 3. (Color online) The charge currents I as a function of the ribbon width N_1 with different magnetic fields ϕ: (a) $\phi = 0.0016$, (b) $\phi = 0.0021$, (c) $\phi = 0.0025$, and (d) $\phi = 0.0028$. Other parameters are the same as in Fig. 2(a). The currents I_1, I_4, and I_5 are almost zero and overlap together.

the left region and the second-electron Landau level of the right region. Similarly, in ϕ_2, the Fermi energy just meets the first-hole Landau level of the left region and the first-electron Landau level of the right region.

When $\phi < \phi_1$, the cyclotron radius is so large that edge states have not formed. So the current from terminal 6 can be scattered into all outgoing terminals, i.e., $I_1,\ldots,I_4$ and I_5 are nonzero, and it is very difficult to observe the regular oscillation of current. When $\phi_1 < \phi < \phi_2$ [see the shaded region in Fig. 2(a)], the cyclotron radius is smaller than the device size, N_1, and edge states have formed. The filling factors in the left and right regions are $(\nu_L,\nu_R) = (-6,6)$. In this region, we can see that the outgoing currents, I_2 and I_3, are evident and the other outgoing currents, I_1, I_4, and I_5, almost vanish. In the beginning, the carriers injected from terminal 6 turn right due to the Lorentz force and travel along the low boundary until they arrive at the p-n interface [see Fig. 1(b)]. Then, the carriers zigzag along the p-n interface through the snake state, and they finally flow into the left terminal 2 or right terminal 3 depending on the final route of snake state. Thus, only the currents I_2 and I_3 are nonzero. If the magnetic field varies with the change of cyclotron radius, the currents I_2 and I_3 exhibit the oscillation behavior, which well indicates the presence of a snake state. Moreover, in a reversed magnetic field [see the inset of Fig. 2(a)], the incident current I_6 is unchanged but the outgoing current I_1 instead of I_2 and I_3 is nonzero, because the carriers injected from terminal 6 turn left and flow into terminal 1 along the low boundary due to the reversed Lorentz force. This gives a strong proof that the above oscillations of I_2 and I_3 are indeed caused by the snake states. In addition, the region with $(\nu_L,\nu_R) = (-6,6)$ is not affected by the width N_1, but the oscillations of the currents I_2 and I_3 are more frequent for the wider ribbon, by comparing the case of $N_1 = 100$ in Fig. 2(b) with that of $N_1 = 60$ in Fig. 2(a), which can be explained well by the snake states too. When $\phi > \phi_2$, the cyclotron radius is small so the snake states will disappear gradually and no evident oscillations of the currents I_2 and I_3 are exhibited in Figs. 2(a) and 2(b), although only I_2 and I_3 are still nonzero. Hereafter, we focus on the region with $(\nu_L,\nu_R) = (-6,6)$, because only outgoing currents I_2 and I_3 exist and the current oscillations can be observed easily.

In the following, the effect of the geometrical structure is investigated. In Fig. 3, the charge currents as a function of the width N_1 are shown in different magnetic fields. For a very narrow graphene ribbon (e.g., small $N_1 < 30$), I_6 varies largely due to strong scattering. However, for a wide ribbon (such as the width $N_1 > 30$ and when the edge states have formed), I_6 does not change anymore. Meanwhile, the periodic structure for I_2 and I_3 occurs and I_1, I_4, and I_5 approach zero. The periodic oscillation holds well and the damping is nearly unseen at least for $N_1 < 200$. There is a phase difference π between the currents I_2 and I_3, i.e., when I_2 reaches its maximum I_3 gets minimum and otherwise, but $I_2 + I_3 \approx I_6$ is almost unchanged with varying width N_1. These results can be explained well by snake states. Here, the oscillation period for the width, T_{N_1}, and the oscillation amplitude decrease with the increasing magnetic field, which is related to the cyclotron radius reduced by a magnetic field as the classical case. Moreover, the period T_{N_1}, the oscillation amplitude, and the width values corresponding the maximums and minimums of I_2 and I_3 are independent of the location of incident terminal 6, L_6, as seen in Fig. 4. In fact, they are also independent of the locations L_2, L_3, and L_5 of terminals 2, 3, and 5 (not shown here), because they are determined only by the relation between the ribbon width and the period of the snake states. L_6 can affect the average magnitude of the currents I_2 and I_3 as shown in Fig. 4, especially for small L_6 (such as $L_6 < 50$).

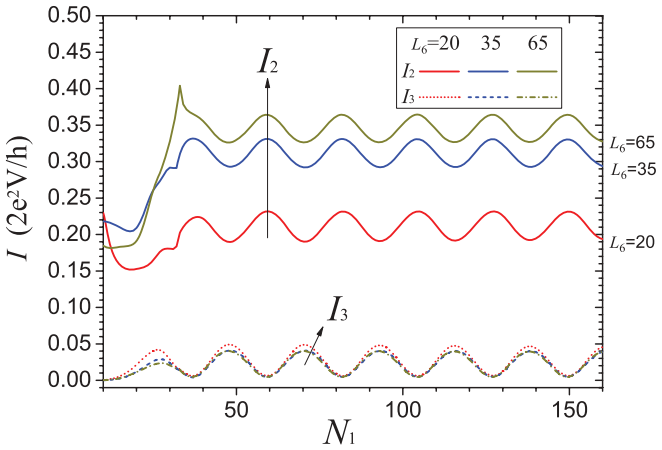

FIG. 4. (Color online) The charge currents I_2 and I_3 as a function of ribbon width N_1 under a fixed magnetic field $\phi = 0.0028$ with different locations of terminal 6. Other parameters are the same as in Fig. 2(a).

However, for $L_6 > 50$, the average magnitude of the currents weakly depends on L_6.

In Fig. 5, the effect of the location of incident terminal 6 on the current oscillation is investigated. Experimentally, the fixed incident terminal 6 can be replaced with the tip of a STM. So it is simple to change the location of the incident terminal by moving the tip of a STM. Here, the periodic oscillations of the currents I_2 and I_3 still hold well and the damping is almost absent. There is a phase difference π between them as well and when I_2 reaches its maximums I_3 reaches its minimums, as seen in Fig. 2(a). The oscillation period of currents with respect to L_6, T_{L_6}, is reduced with increasing magnetic field, which is similar to the case of T_{N_1}. But the oscillation amplitudes are related to the special magnetic field. In Figs. 5(b) and 5(d) for $\phi = 0.0021$ and 0.0028, I_2 is located near its maximum in Fig. 2(a); i.e., the current from terminal

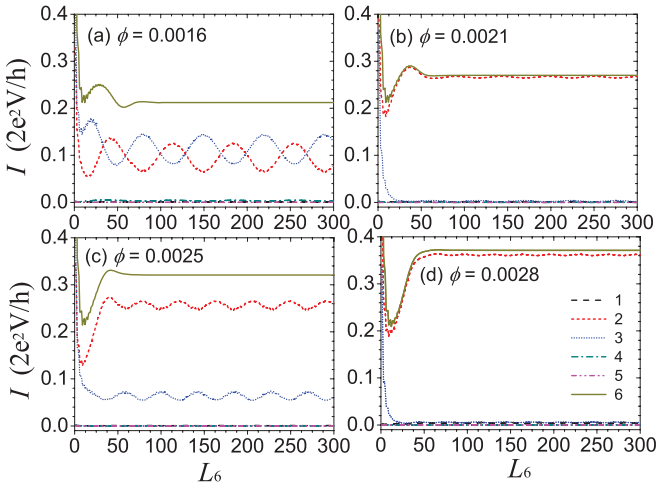

FIG. 5. (Color online) The charge currents I as a function of the location of terminal 6, L_6, with different magnetic fields: (a) $\phi = 0.0016$, (b) $\phi = 0.0021$, (c) $\phi = 0.0025$, and (d) $\phi = 0.0028$. The legend in (d) is for all panels. Other parameters are the same as in Fig. 2(a). The currents I_1, I_4, and I_5 are almost zero and overlap together.

6 almost flows into the terminal 2. From the viewpoint of the classical route of the snake state, the ribbon width N_1 is just equal to an integer multiple of T_{N_1} ($N_1 = nT_{N_1}$ with $n = 1,2,\ldots$). Thus, the final route of carriers will arrive at the left side on the top corner of the p-n interface, as long as the carriers collide with the p-n interface from its left side on the bottom corner. Hence, the current always flows into terminal 2 and the oscillation amplitudes of the currents I_2 and I_3 are small. On the other hand, in Fig. 5(c) for $\phi = 0.0025$, I_2 is located near its minimum in Fig. 2(a), which means that the ribbon width N_1 is equal to a half-integer multiple of T_{N_1} [$N_1 = (n + 1/2)T_{N_1}$ with $n = 1,2,\ldots$]. In this case, the oscillation amplitudes are large.

IV. PERIODS OF CURRENT OSCILLATION

Next, in order to further investigate the periodic structure of the current oscillation, we extract the values of the ribbon width N_1 and the location of incident terminal L_6 corresponding to the maximums of I_2.

In Fig. 6, we extract the values of the width N_1 corresponding the maximums of I_2 from Fig. 3 and these widths are plotted in order where the abscissa n denotes the sequence of maximums of I_2. For each case of Fig. 6, the dots can be well arranged into a straight line, which indicates that the periodicity of the oscillation keeps very well and the

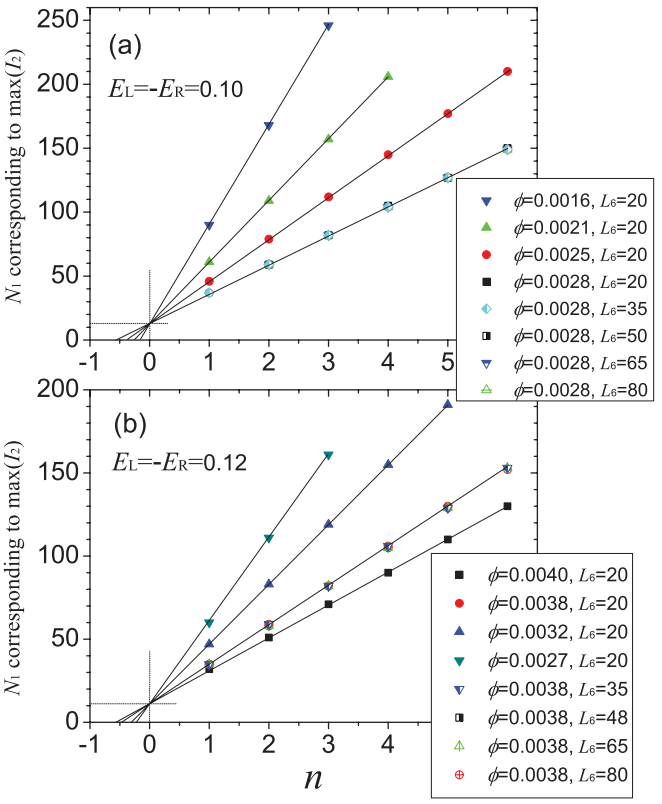

FIG. 6. (Color online) The values of the ribbon width N_1 correspond to the maximums of current I_2 with different magnetic fields ϕ and the locations of terminal 6, L_6, for two on-site energies, (a) $E_L = -E_R = 0.10$ and (b) 0.12. The abscissa n denotes the sequence number of maximums of I_2. Other unmentioned parameters are the same as in Fig. 2(a).

slope of each line is the corresponding period. In Fig. 6(a), with increasing magnetic field with fixed L_6, the slopes of the straight lines decrease; i.e., the periods T_{N_1} decrease. It is surprising that all lines cross a point, which corresponds $n = 0$ and the width $N_1 = 13$ (≈5.54 nm). This cross point is not located at the origin point, which indicates the width $N_1 = nT_{N_1}$ does not correspond the maximums of I_2. From the classical route of the snake state, these lines should be $N_1 = nT_{N_1}(\phi)$ and all lines should cross at the origin point. This deviation from the origin point results because the snaky periods of the snake state near the bottom and top edges of the sample are slightly different from that in the middle of the sample due to the edge effect. For different L_6 with fixed magnetic field, all the lines overlap (i.e., the period T_{N_1} is unchanged with varying location of terminal 6). Moreover, the above observation occurs for other barrier heights, such as $E_L = -E_R = 0.12$ in Fig. 6(b). The lines with different magnetic fields still cross a point at $n = 0$ but the corresponding width N_1 is about 11 now.

In addition, in Fig. 7(a), the values of L_6 corresponding to the maximums of the current I_2 are extracted from Fig. 5 for different magnetic fields. Similar to the case for the ribbon width N_1, the dots can be well arranged into a straight line in each case of Fig. 7 and the slopes (i.e., the periods T_{L_6}) decrease with increasing magnetic field. All lines cross a point, where L_6 is about 25 (≈6.1 nm) but $n \neq 0$. The position of the

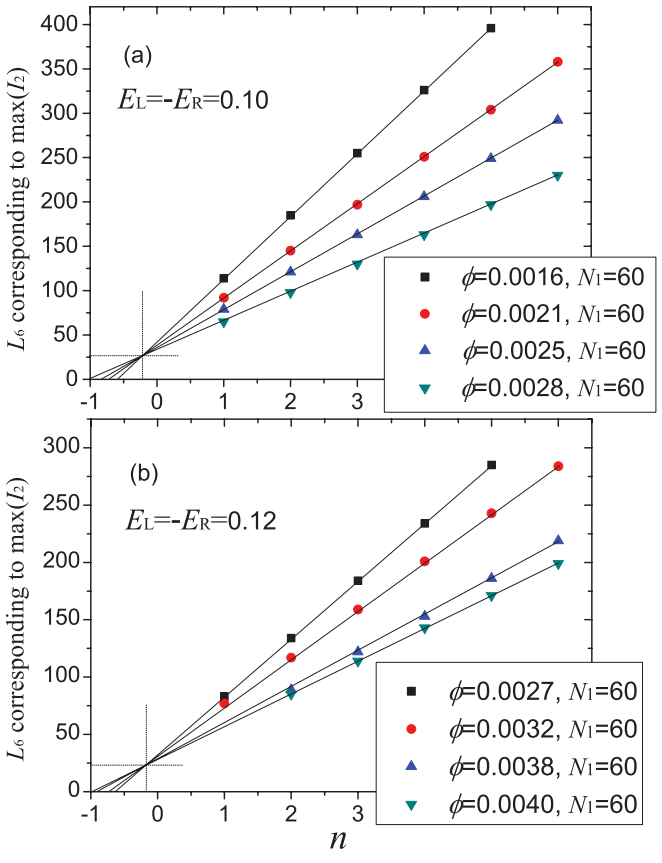

FIG. 7. (Color online) The values of the location of terminal 6, L_6, correspond to the maximums of the current I_2 with different magnetic fields ϕ for two on-site energies, (a) $E_L = -E_R = 0.10$ and (b) 0.12. Other unmentioned parameters are the same as in Fig. 2(a).

cross point infers that $L_6 = nT_{L_6}$ does not correspond to the maximums of I_2 as well. For the other barrier height, a similar phenomenon can be observed, such as for $E_L = -E_R = 0.12$ in Fig. 7(b).

Furthermore, the oscillation periods of currents with respect to N_1 and L_6, T_{N_1} and T_{L_6}, which are extracted from the slopes in Figs. 6 and 7, are plotted as a function of magnetic field in Fig. 8(a). By intuition, the cyclotron radius r is a constant under a fixed magnetic field. Then, $T_{N_1} = 4r$, $T_{L_6} = 2r$, and the rate of them is $T_{N_1}/T_{L_6} = 2$ regardless of the magnetic field. However, in Fig. 8(a), it is found that the rate T_{N_1}/T_{L_6} is not a constant and it decreases with increasing magnetic field ϕ. The reason should be that the carriers need to travel along the ribbon boundary with a zigzag edge but along the p-n interface with an armchair edge, so they have different cyclotron radii. The rate T_{N_1}/T_{L_6} is about 2 when the magnetic field ϕ is in the vicinity of ϕ_1, and it gradually decreases to 1 as ϕ increases to ϕ_2.

In semiclassical theory, the effective cyclotron radius is given as[2–4]

$$r = \frac{m_c^* v}{eB}, \tag{3}$$

where v is the group velocity of carriers in graphene and m_c^* is an effective cyclotron mass defined as $\frac{\hbar^2}{2\pi}[\frac{\partial A(E)}{\partial E}]_{E=E_F}$ with $A(E)$ the area in two-dimensional k space enclosed by the orbit. However, in the present case, two difficulties occur in the calculation of the effective cyclotron mass m_c^*: (i) The Fermi energy E_F is located between two Landau levels; thus, the bulk states on the Fermi energy are insulating and we cannot obtain the area $A(E_F)$. (ii) For the one-dimensional band structure of a nanoribbon, the area $A(E)$ cannot be obtained either. In the following, we adopt two methods to roughly estimate the effective cyclotron mass m_c^* and then cyclotron radius: (i) The effective cyclotron mass m_c^* is replaced with the effective mass m^*, which can be obtained from the one-dimensional (1D) band structure of a nanoribbon[32]

$$m^* = \frac{\hbar^2}{\partial^2 E/\partial k^2} \quad \text{and} \quad v = \frac{1}{\hbar}\frac{\partial E}{\partial k}, \tag{4}$$

where E is the energy and k is the wave vector. Here, three effective masses m^* and then effective radiuses r_{z1}, r_{z2}, and r_{z3} (r_{a1}, r_{a2}, and r_{a3}) can be calculated from cross points between the Fermi energy and the energy bands of a zigzag (armchair) nanoribbon [see Figs. 8(b) and 8(c)]. For a zigzag (armchair) ribbon, one of these three points originates from the zeroth Landau level and the other two from the first Landau level. Thus, r_{z1} and r_{a1}, corresponding to the zeroth Landau level, are neglected for discussion, and we consider r_{z2}, r_{z3}, r_{a2}, and r_{a3} only; r_{z2} and r_{z3} are almost equal to each other but r_{a2} and r_{a3} have some differences. Here we adopt $\bar{r}_z = (r_{z2} + r_{z3})/2$ and $\bar{r}_a = (r_{a2} + r_{a3})/2$. In Fig. 8(a), we find that $\bar{r}_z$ and $\bar{r}_a$ decrease with the increase of the magnetic field. This tendency with varying magnetic field as well as the order of magnitude of $2\bar{r}_z$ and $2\bar{r}_a$ ($4\bar{r}_z$ and $4\bar{r}_a$) is the same as that of T_{L_6} (T_{N_1}). But the specific magnitudes among them are not identical to each other. This departure may result because the effective mass and velocity in Eq. (4) are described semiclassically in the case of a carrier accelerated by an electrostatic field. But the carriers advance actually along a spiral, not a straight,

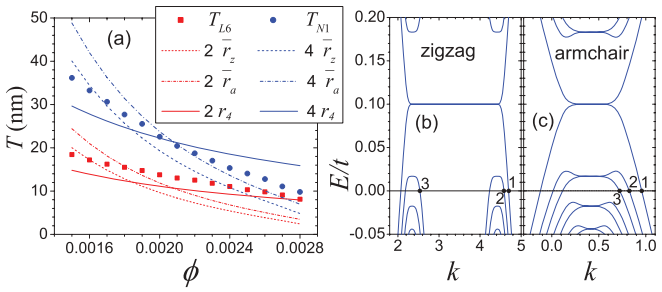

FIG. 8. (Color online) (a) Dots are the oscillation periods with respect to N_1 and L_6, T_{N_1} and T_{L_6}, as a function of magnetic field. The radii $\bar{r}_z$, $\bar{r}_a$, and r_4 are explained in the text. Other unmentioned parameters are the same as in Fig. 2(a). The energy-band structures are shown for (b) the zigzag graphene ribbon of width $N_1 = 60$ and (c) the armchair graphene ribbon of the same width as (b).

trajectory, due to the Lorentz force by the magnetic field. (ii) We make use of the relation $m_c^* = |\Delta E|/v^2$, where $|\Delta E|$ is an energy separation between the Dirac point and the Fermi energy, which has been confirmed for low energy around the Dirac point from experiments.[2,3] Then, Eq. (3) can be written as

$$r_4 = \frac{|\Delta E|}{veB}, \tag{5}$$

where $v \approx 10^6$ m/s. In Fig. 8, the curves of $2r_4$ and $4r_4$ versus the magnetic field ϕ are also plotted. We find that the order of magnitude of $2r_4$ ($2r_4$) as well as its tendency with varying magnetic field is the same as that of T_{L_6} (T_{N_1}), although they still have some differences. In this case, the departure may be caused because the linear dispersion of low energy is distorted by the magnetic field and the relation $|\Delta E| = m_c^* v^2$ is no longer satisfied.

V. EFFECT OF SMOOTH POTENTIAL BARRIER ON THE SNAKE STATES

In the experiment, the potential barrier across the p-n junction is usually not a sharp step but smooth. In Fig. 9, the effect of smooth potential barriers on the current oscillation is investigated. Here, we consider two smooth potential barriers, the sine potential and the linear potential, as shown in the inset

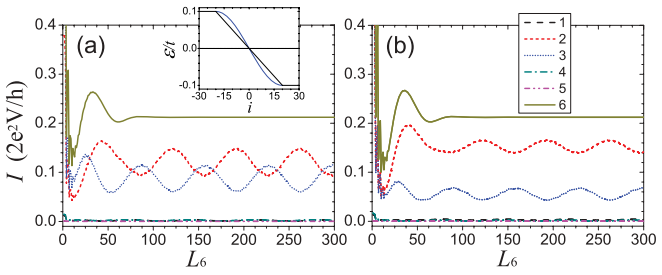

FIG. 9. (Color online) The currents I as a function of L_6 for smooth potential barriers: (a) sine potential and (b) linear potential. Inset of (a): the figures of the potential distribution. Other unmentioned parameters are the same as in Fig. 5(a). The currents I_1, I_4, and I_5 are almost zero and overlap together.

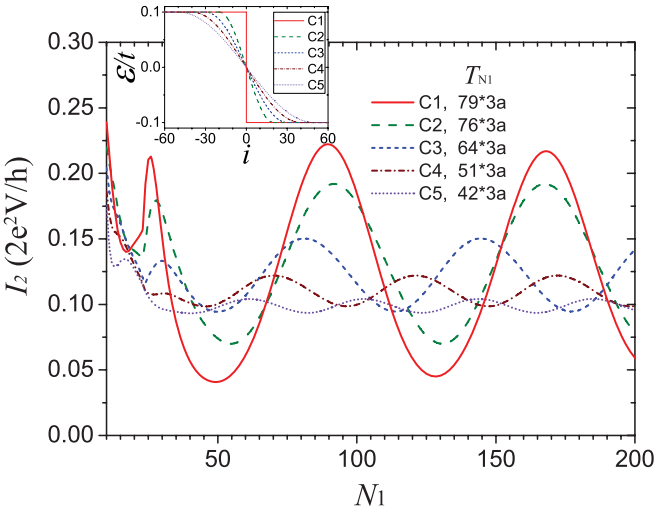

FIG. 10. (Color online) The current I_2 as a function of N_1 for different sine potential barriers. Inset: the figures of the potential distribution. The parameters $N_2 = 60$, $N_6 = 3$, $L_2 = L_3 = L_5 = L_6 = 20$, and $\phi = 0.0016$ are the same as in Fig. 3(a).

of Fig. 9(a). When the potential barrier is smooth, the on-site energy ϵ_i in the region between terminal 2 and terminal 3, i.e., between L_2 and L_3 [see Fig. 1(a)], is changed slowly. For the sine potential case, $\epsilon_i = -E_L \sin(i\pi/(L_2 + L_3))$, and for the linear potential case, $\epsilon_i = E_L - (E_L - E_R)(i + L_2)/(L_2 + L_3)$, where $-L_2 \leqslant i \leqslant L_3$ and i is the column index.

Figures 9(a) and 9(b) show the currents versus the location of the incident terminal 6 for the sine potential and linear potential, respectively. For the same parameters but with the sharp step potential, these currents are shown in Fig. 5(a). We find that the periodic oscillation of the currents can still survive. By comparing the case of the smooth potential with the sharp step potential, the oscillation periods and the locations of maximums (minimums) of currents I_2 and I_3 are almost unchanged. For the sine potential case, the oscillation amplitude is almost the same as that of the sharp step potential, and for the linear potential case, the oscillation amplitude is slightly reduced.

In addition, Fig. 10 shows the current I_2 versus the width of the nanoribbon, N_1, for different sine potential barriers. The current oscillations still hold, but their periods T_{N_1} and amplitudes decrease as the potential extends gradually. In a smooth potential, the closer the positions are to the p-n interface, the smaller the energy separation between Fermi energy and Dirac point $|\Delta E|$ is. According to Eq. (5), their cyclotron radius is smaller. So the smooth potential reduces the period T_{N_1} of a snake state traveling along the interface.

Furthermore, these periodic oscillation of the currents in Figs. 9 and 10 can remain to be clearly observed until the smooth potential extends to a very large range, about $-150 \lesssim i \lesssim 150$, in which the corresponding length of the change of potential is $300\sqrt{3}a \approx 74$ nm. In the experiment, it is more convenient to move the tip of a STM instead of varying the incident terminal 6 than to change the width of the nanoribbon. Hence, these current oscillations and the presence of the snake states can be observed experimentally by present technology.

VI. CONCLUSION

In summary, we have investigated the snake states in a six-terminal graphene *p-n* junction under a perpendicular magnetic field. The current oscillation with varying magnetic field appears due to the presence of snake states at the *p-n* interface. The periodic properties of currents with respect to the geometric structures, such as the width and the location of the incident terminal, are also shown. Two emerging periods decrease with increasing magnetic field, but the rate between them is not simply equal to 2, as predicted by a simple theory. In addition, the oscillation amplitude and the locations of the oscillation maximums and minimums are investigated. Finally, for a smooth potential, the snake states and the current oscillations still survive. We conclude that the snake states should be experimentally observable in the proposed device.

ACKNOWLEDGMENTS

This work was financially supported by NBRP of China (2012CB921303 and 2009CB929100), NSF-China, under Grants No. 10974236, No. 11074174, and No. 11121063.

*sunqf@iphy.ac.cn

[1] K. S. Novoselov, A. K. Geim, S. V. Morozov, D. Jiang, Y. Zhang, S. V. Dubonos, I. V. Grigorieva, and A. A. Firsov, Science **306**, 666 (2004).

[2] K. S. Novoselov, A. K. Geim, S. V. Morozov, D. Jiang, M. I. Katsnelson, I. V. Grigorieva, S. V. Dubonos, and A. A. Firsov, Nature (London) **438**, 197 (2005).

[3] Y. Zhang, Y.-W. Tan, H. L. Stormer, and P. Kim, Nature (London) **438**, 201 (2005).

[4] A. H. C. Neto, F. Guinea, N. M. R. Peres, K. S. Novoselov, and A. K. Geim, Rev. Mod. Phys. **81**, 109 (2009).

[5] J. R. Williams, L. DiCarlo, and C. M. Marcus, Science **317**, 638 (2007).

[6] T. Lohmann, K. V. Klitzing, and J. H. Smet, Nano Lett. **9**, 1973 (2009).

[7] L. DiCarlo, J. R. Williams, Y. Zhang, D. T. McClure, and C. M. Marcus, Phys. Rev. Lett. **100**, 156801 (2008).

[8] R. V. Gorbachev, A. S. Mayorov, A. K. Savchenko, D. W. Horsell, and F. Guinea, Nano Lett. **8**, 1995 (2008).

[9] B. Huard, J. A. Sulpizio, N. Stander, K. Todd, B. Yang, and D. Goldhaber-Gordon, Phys. Rev. Lett. **98**, 236803 (2007).

[10] B. Özyilmaz, P. Jarillo-Herrero, D. Efetov, D. A. Abanin, L. S. Levitov, and P. Kim, Phys. Rev. Lett. **99**, 166804 (2007).

[11] N. Stander, B. Huard, and D. Goldhaber-Gordon, Phys. Rev. Lett. **102**, 026807 (2009).

[12] V. V. Cheianov, V. Fal'ko, and B. L. Altshuler, Science **315**, 1252 (2007).

[13] Y. Xing, J. Wang, and Q.-F. Sun, Phys. Rev. B **81**, 165425 (2010).

[14] C. W. J. Beenakker, Rev. Mod. Phys. **80**, 1337 (2008).

[15] M. I. Katsnelson, K. S. Novoselov, and A. K. Geim, Nat. Phys. **2**, 620 (2006).

[16] V. V. Cheianov and V. I. Fal'ko, Phys. Rev. B **74**, 041403 (2006).

[17] L. Oroszlány, P. Rakyta, A. Kormányos, C. J. Lambert, and J. Cserti, Phys. Rev. B **77**, 081403 (2008).

[18] T. K. Ghosh, A. DeMartino, W. Hausler, L. Dell'Anna, and R. Egger, Phys. Rev. B **77**, 081404 (2008).

[19] J. E. Müller, Phys. Rev. Lett. **68**, 385 (1992).

[20] N. Davies, A. A. Patel, A. Cortijo, V. Cheianov, F. Guinea, and V. I. Fal'ko, Phys. Rev. B **85**, 155433 (2012).

[21] J. R. Williams and C. M. Marcus, Phys. Rev. Lett. **107**, 046602 (2011).

[22] L. W. Molenkamp, A. A. M. Staring, C. W. J. Beenakker, R. Eppenga, C. E. Timmering, J. G. Williamson, C. J. P. M. Harmans, and C. T. Foxon, Phys. Rev. B **41**, 1274 (1990).

[23] K. E. Aidala, R. E. Parrott, T. Kramer, E. J. Heller, R. M. Westervelt, M. P. Hanson, and A. C. Gossard, Nat. Phys. **3**, 464 (2007).

[24] A. Cresti, N. Nemec, B. Biel, G. Niebler, F. Triozon, G. Cuniberti, and S. Roche, Nano Res. **1**, 361 (2008).

[25] J.-C. Chen, H. Zhang, S.-Q. Shen, and Q.-F. Sun, J. Phys.: Condens. Matter **23**, 495301 (2011).

[26] J. Li and S.-Q. Shen, Phys. Rev. B **78**, 205308 (2008).

[27] J.-C. Chen, T. C. A. Yeung, and Q.-F. Sun, Phys. Rev. B **81**, 245417 (2010).

[28] W. Long, Q.-F. Sun, and J. Wang, Phys. Rev. Lett. **101**, 166806 (2008).

[29] S. Datta, *Electronic Transport in Mesoscopic Systems* (Cambridge University Press, Cambridge, 1995).

[30] M. P. Lopez Sancho, J. M. Lopez Sancho, J. M. L. Sancho, and J. Rubio, J. Phys. F **15**, 851 (1985).

[31] A. Cresti, G. Grosso, and G. P. Parravicini, Phys. Rev. B **77**, 115408 (2008).

[32] N. W. Ashcroft and N. D. Mermin, *Solid State Physics* (Holt, Rinehart and Winston, New York, 1976).